Studies of a linear single-molecule magnet†

Alessandro Prescimone,[a] Joanna Wolowska,[b] Gopalan Rajaraman,[b] Simon Parsons,[a] Wolfgang Wernsdorfer,[c] Murlaee Murugesu,[d] George Christou,[d] Stergios Piligkos,[e] Eric J. L. McInnes*[b] and Euan K. Brechin*[a]

Received 28th August 2007, Accepted 25th September 2007
First published as an Advance Article on the web 15th October 2007
DOI: 10.1039/b713163a

Reaction of the dinuclear complex $[Mn_2O_2(bpy)_4](ClO_4)_3$ with H_3cht (*cis*,*cis*-1,3,5-cyclohexanetriol) in MeCN produces the complex $[Mn_3(Hcht)_2(bpy)_4](ClO_4)_3{\cdot}Et_2O{\cdot}2MeCN$ (**1**·Et_2O·2MeCN). Dc magnetic susceptibility measurements reveal the existence of weak ferromagnetic exchange between the three Mn ions, leading to a spin ground state of $S = 7$, with $D = -0.23$ cm^{-1}. W-Band (94 GHz) EPR measurements on restrained powdered crystalline samples confirm the $S = 7$ ground state and determine the ground state zero-field splitting (ZFS) parameters of $D = -0.14$ cm^{-1} and $B_4^0 = +1.5 \times 10^{-5}$ cm^{-1}. The apparent 4th order behaviour is due to a breakdown of the strong exchange limit approximation ($J \approx d$, the single-ion ZFS). Single crystal dc relaxation decay and hysteresis loop measurements reveal the molecule to have an appreciable energy barrier to magnetization relaxation, displaying low temperature sweep rate and temperature-dependent hysteresis loops. Density functional studies confirm the ferromagnetic exchange coupling between the Mn ions.

Introduction

Since various specialized applications of magnets require monodisperse, small magnetic particles, the discovery of molecules that can function as nanoscale magnets was an exciting development.[1–5] These molecules, called single-molecule magnets (SMMs),[6] exhibit the classical properties of a macroscopic magnet below their blocking temperature,[3,4] which is currently limited to about 5 K. Because of their small size, SMMs have also been shown to exhibit interesting phenomena belonging to the quantum world, such as quantum tunneling of magnetization[7–9] and quantum phase interference[9,10]—key properties needed for materials to function as quantum bits (qubits).[11] The most thoroughly studied SMMs are members of the $[Mn_{12}O_{12}(O_2CR)_{16}(H_2O)_4]$ (Mn_{12}) family,[1,3–5] since—until recently—they represented the family of molecules with the largest blocking temperatures. In 2007 this record was broken by the family of molecules of general formula $[Mn_6O_2(Et\text{-}sao)_6(O_2CR)_2(ROH)_4]$, all of which are characterized by $S = 12$ ground states and anisotropies of the order -0.43 cm^{-1}.[12]

For some time, we have been exploring the reactivity of tripodal alcohols (Scheme 1) in the synthesis of 3d transition metal SMMs.[13] When fully deprotonated the disposition of the three alkoxide arms of the tri-anion generally directs the formation of triangular $[M_3]$ units where each arm of the ligand bridges one edge of the triangle. In the presence of co-ligands such as carboxylates or β-diketonates *etc.*, these smaller units can combine in diverse ways to produce complexes whose structures range from 'simple' $[M_3]$ or $[M_4]$ (centered) triangles to rod-like complexes describing 'one dimensional' arrays of edge-sharing triangles; planar disc-like complexes describing 'two dimensional' arrays of edge-sharing triangles; and more complicated 'three dimensional' arrays commonly based on tetrahedra, octahedra and icosahedra.[13] However, when the three arms are not fully deprotonated (*i.e.* H_2tripod$^-$, Htripod^{2-}) the resultant complexes and their metallic skeletons have much less predictable topologies—and have even been shown to form wheels.[14] The majority of the complexes we have isolated have employed either 1,1,1-tris(hydroxymethyl)ethane (H_3thme), 1,1,1-tris(hydroxymethyl)propane (H_3tmp), or pentaeryrithritol (H_4peol) and, in general (though certainly not always), each produces similar molecules, differing more in their inter-molecular interactions and crystal packing than their intra-molecular bonding. A natural extension to this is the study of the coordination chemistry of *cis*,*cis*-1,3,5-cyclohexanetriol (H_3cht, Scheme 1)—and initial results suggest there may indeed be some significant differences. While there are a number of monometallic complexes based on H_3cht, polymetallic clusters are extremely rare—indeed there are only two examples: the decametallic Ni supertetrahedron $[Ni_{10}O_6(cht)_4(O_2CMe)_2(dpm)_4(H_2O)_2]$ (where hdpm = dipivaloylmethane) we reported in 2004[15] and the trimetallic Ti(IV) complex $[Ti_3(cht)_2(O^iPr)_6]$ reported in 1999.[16]

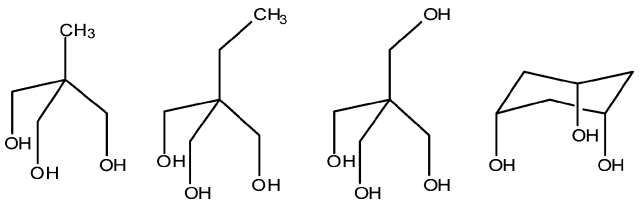

Scheme 1 The tripodal alcohols (left to right) 1,1,1-tris(hydroxymethyl)-ethane, H_3thme; 1,1,1-tris(hydroxymethyl)propane, H_3tmp; pentaerythritol, H_4peol; *cis*,*cis*-1,3,5-cyclohexanetriol, H_3cht.

[a]*School of Chemistry, University of Edinburgh, West Mains Road, Edinburgh, UK EH9 3JJ. E-mail: ebrechin@staffmail.ed.ac.uk; Tel: +44-(0)131-650-7545*
[b]*EPSRC Multi-frequency EPR Service, School of Chemistry, The University of Manchester, Oxford Road, Manchester, UK M13 9PL. E-mail: eric.mcinnes@manchester.ac.uk*
[c]*Institut Néel–CNRS, 38042 Grenoble, Cedex 9, France*
[d]*Chemistry Department, University of Florida, Gainesville, Florida, 32611-7200, USA*
[e]*Department of Chemistry, University of Copenhagen, Universitetsparken 5, DK-2100, Denmark*

† Electronic supplementary information (ESI) available: In-phase ac susceptibility plot and W-band EPR spectra for complex **1**. See DOI: 10.1039/b713163a

 This journal is © The Royal Society of Chemistry 2007

Here we describe the synthesis, structure and magnetic properties of the first polynuclear Mn complex based on H_3cht, a rare example of a linear Mn complex, and the first example of a trimetallic SMM.[17a,b]

Experimental

All manipulations were performed under aerobic conditions, using materials as received. $[Mn_2O_2(bpy)_4](ClO_4)_3$ was prepared as previously described.[17c]

$[Mn_3(Hcht)_2(bpy)_4](ClO_4)_3{\cdot}Et_2O{\cdot}2MeCN$ (**1**·Et_2O·2MeCN). to a stirred solution of $[Mn_2O_2(bpy)_4](ClO_4)_3$ (2 mmol) in CH_3CN (30 ml) was added solid H_3cht (2 mmol). The resulting dark brown suspension was left stirring overnight, during which time it changed colour to orange-brown. The solution was filtered and layered with two volumes of Et_2O. After three days the orange crystals formed were isolated by filtration, washed with Et_2O and dried *in vacuo*; yield ~45%. A sample for X-ray crystallography was kept in the mother liquor to prevent solvent loss. Anal. Calcd (found) for **1**·0.5MeCN, $Mn_3C_{53}H_{53.5}N_{4.5}O_{18}Cl_3$: C, 48.01 (47.95); H, 4.12 (4.02); N, 4.85 (4.79)%.

Physical methods

Elemental analyses (C, H, N) were performed by the EaStCHEM microanalysis service. Variable-temperature, solid-state direct current (dc) magnetic susceptibility data down to 1.80 K were collected on a Quantum Design MPMS-XL SQUID magnetometer equipped with a 7 T dc magnet. Diamagnetic corrections were applied to the observed paramagnetic susceptibilities using Pascal's constants. Magnetization *versus* field hysteresis and dc decay measurements at temperatures below 1.8 K were performed on single crystals using a micro-SQUID instrument.[18]

EPR spectra were measured at Q- and W-band on Bruker ESP 300E and Elexsys spectrometers, respectively. For W-band measurements it was necessary to restrain polycrystalline samples of **1** in eicosane wax in order to prevent torquing in the applied magnetic fields. Simulations were performed with Weihe's "SimEPR" software.[19]

X-Ray crystallography and structure solution: crystals were kept in contact with the mother liquor to avoid solvent loss and were crystallographically identified as **1**·Et_2O·2MeCN. Diffraction data were collected with Mo-Kα X-radiation ($\lambda = 0.71073$ Å) on a Bruker Smart APEX diffractometer equipped with an Oxford Cryosystems low-temperature device operating at 150 K. An absorption correction was applied using the program SADABS;[20] the structure was solved using Patterson methods (DIRDIF)[21] and refined by full-matrix least squares against F^2 (SHELXTL)[20] using all unique data. Crystal data: $C_{60}H_{68}Mn_3Cl_3N_{10}O_{19}$, $M = 1504.41$, orange blocks, monoclinic, $I2/m$, $a = 11.919(2)$, $b = 22.044(4)$, $c = 13.385(2)$ Å, $\beta = 96.863(4)°$, $V = 3491.6(10)$ Å^3, 14880 reflections measured, of which 3915 were independent, $\theta_{max} = 27.04°$, 901 parameters and 13 restraints, $R = 0.0953$ [based on $F > 4\sigma(F)$], $Rw = 0.2653$ (based on F^2 and all data). CCDC 263449.

Exchange coupling constants were estimated computationally using the program Jaguar,[22] with the calculations performed with the hybrid B3LYP functional.[23–25] Double-ζ (SV) and triple-ζ (TZV) (for the Mn atoms) quality basis sets proposed by Ahlrichs and co-workers were used, since this combination has been shown to provide a good estimate of magnetic exchange interactions.[26–28]

Results and discussion

Synthesis and structure description

Reaction of the dinuclear complex $[Mn_2O_2(bpy)_4](ClO_4)_3$ with one equivalent of H_3cht in MeCN initially produces a dark brown solution. The H_3cht is reasonably insoluble in MeCN but as the reaction proceeds and the H_3cht dissolves, distinctive colour changes occur: firstly to light brown, then to red-brown and finally orange-brown, over a period of approximately 12 h. Orange crystals of $[Mn_3(Hcht)_2(bpy)_4](ClO_4)_3{\cdot}Et_2O{\cdot}2MeCN$ (**1**·Et_2O·2MeCN) are obtained upon diffusion of diethyl ether into this orange-brown solution during three days. The synthesis of complex **1** can be regarded as a '*reductive aggregation*'—a process whereby a high oxidation state Mn source is deliberately reacted in conditions that force a reduction of the metal centre(s) and a concomitant structural rearrangement (in the presence or absence of (additional) bridging ligands) that results in the formation of a new product. Here the reduction of the metal centre(s) ($Mn^{IV}Mn^{III}$ to $Mn^{III}Mn^{II}{}_2$) is accompanied by the double deprotonation of the tripodal alcohol (H_3cht to $Hcht^{2-}$). Clearly, as is the case with almost all Mn cluster chemistry, complex **1** is unlikely to be the only species present and its formation and crystallization is an extremely complicated process which also involves the protonation/deprotonation, structural rearrangement and redox chemistry of many other species present in solution. Reductive aggregation using high-oxidation state Mn precursors is an excellent, yet still underused, method for synthesizing multiple Mn(III)-containing clusters that are of vital importance for the manufacture of high spin molecules with significant magnetoanisotropies.

Complex **1** (Fig. 1) crystallizes in the monoclinic space group $I2/m$, and has crystallographic C_{2h} point symmetry with the C_2

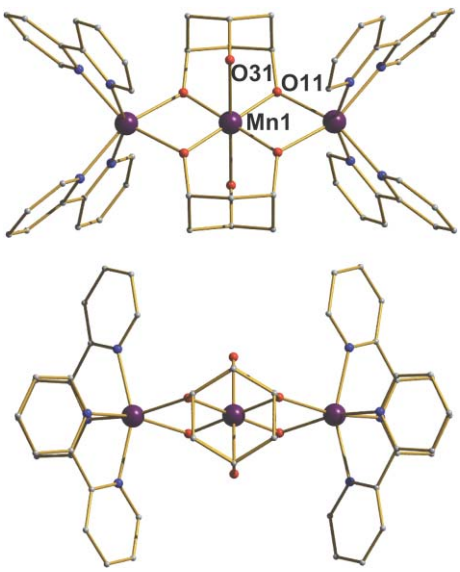

Fig. 1 The molecular structure of the cation of **1**, viewed perpendicular (top) and parallel (bottom) to the $[Mn_3]$ 'plane'. Colour code: Mn = purple, O = red, N = blue, C = grey.

Table 1 Selected bond lengths (Å) and angles (°) for complex **1**

Mn(1)–O(11)	1.898(3)
Mn(1)–O(31)	2.330(7)
Mn(1)–Mn(2)	3.1436(11)
Mn(2)–O(11)	2.142(3)
Mn(2)–N(122)	2.243(4)
Mn(2)–N(12)	2.270(4)
O(11)#1–Mn(1)–O(11)#2	180.0
O(11)#1–Mn(1)–O(11)#3	83.6(2)
O(11)#2–Mn(1)–O(11)#3	96.4(2)
O(11)#1–Mn(1)–O(31)	82.27(15)
O(11)#2–Mn(1)–O(31)	97.73(15)

axis along the Mn···Mn···Mn vector. Selected bond lengths and angles are given in Table 1. The metallic core of the complex comprises a linear $[Mn^{III}Mn^{II}_2O_4]^{3+}$ unit in which the central Mn ion (Mn1) is the sole Mn(III) ion. The metal ions are linked together by four μ-oxygens (O11 and symmetry equivalents) from the two $Hcht^{2-}$ ligands which sit directly, one above and one below, the $[Mn_3]$ plane. The Mn–O–Mn bridging angle is 102°. The third oxygen atom (O31 and symmetry equivalent) of the ligand remains protonated (H-bonding the N atom of the MeCN solvent molecule) and is terminally bound, defining the direction of the Jahn–Teller axis of Mn1. The coordination of the peripheral Mn(II) ions is completed by two chelating bpy molecules. These Mn ions are in distinctly distorted octahedral geometries with *cis* angles in the range 72.30(16)–105.65(15)° and *trans* angles in the range 156.0(2)–158.17(14)°. The bond lengths for the Mn(II) ions lie in the range 2.142(4)–2.270(4) Å while the central Mn(III) ion has four short bonds of 1.898(3) Å in length and two longer bonds of 2.330(7) Å. The oxidation states of both were confirmed by bond valence sum calculations which are summarised in Table 2.

In the crystal the cations pack directly upon each other in such a way that each of the four corners of the unit cell are defined by the central Mn (Mn1) ion of the $[Mn_3]$ molecule, with a $[Mn_3]$ cluster at the centre of the cell. When viewed perpendicular to the *bc* plane the result is an attractive 2D mosaic of $[Mn_3]$ cations that somewhat resembles a honeycomb-type lattice (Fig. 2). The MeCN solvent is H-bonded to the terminal arm of the tripodal ligand (N···O, ~2.8 Å); and the perchlorate ions, which lie between the bpy groups on adjacent $[Mn_3]$ molecules, are H-bonded to the ring carbon atoms (O···H–C, ≥2.3 Å). The closest inter-molecular contacts between the cations occur between off-set 'π-stacked' bpy groups (C···C, >~3.5 Å).

Dc susceptibility

Variable temperature dc magnetic susceptibility data were collected on **1** (Fig. 3) in the temperature range 300–5 K in an applied field of 0.1 T. The room temperature $\chi_M T$ value of approximately 12.3 cm^3 K mol^{-1} slowly increases upon cooling to ~75 K where it then increases rapidly to a maximum value of 21.8 cm^3 K mol^{-1} at 5 K. The spin only ($g = 2$) value for a $[Mn^{III}Mn^{II}_2]$ unit is approximately 12 cm^3 K mol^{-1}. This behaviour is indicative of ferromagnetic exchange between the metal centres resulting in an $S = 7$ ground state. Inspection of the molecular structure reveals the presence of only one exchange interaction (J) between the central Mn(III) ion (Mn1) and the two peripheral Mn(II) ions (Mn2 and symmetry equivalents) mediated *via* the μ-bridging alkoxides.

Table 2 Bond valence sum (BVS) calculations for the metal ions in complex **1**

	Mn^{2+}	Mn^{3+}	Mn^{4+}	Assignment
Mn1	3.45	3.18	3.09	Mn^{3+}
Mn2	1.91	1.75	1.70	Mn^{2+}

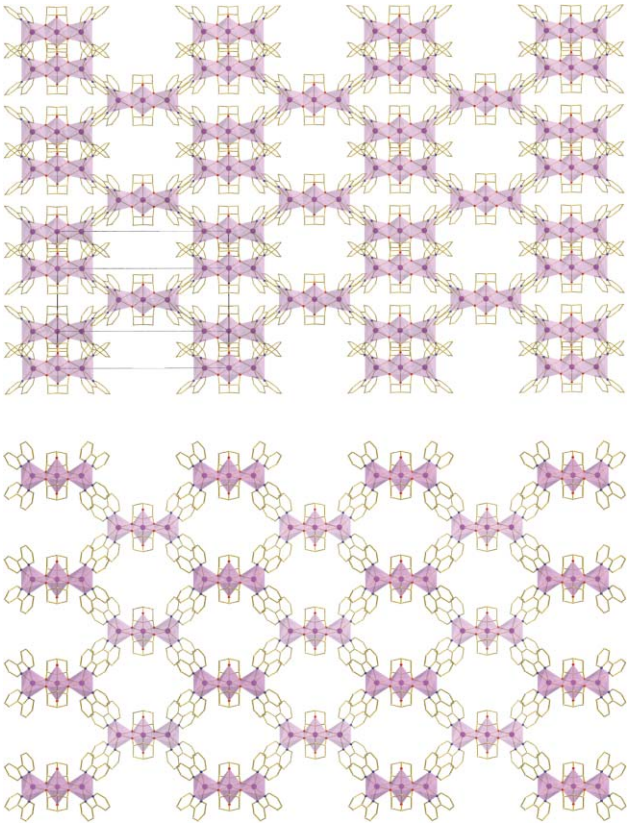

Fig. 2 The packing of the cations of **1** in the crystal, highlighting the unit cell (top), and viewed perpendicular to the *bc* plane (bottom). The anions and solvent have been removed for clarity.

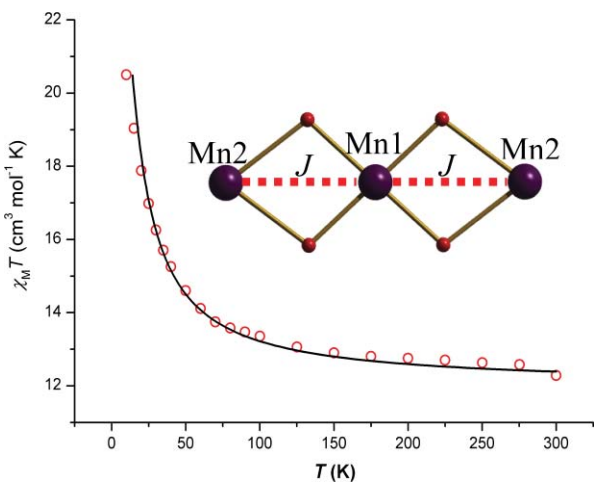

Fig. 3 Plot of $\chi_M T$ *versus* T for complex **1** in the temperature range 300–5 K in an applied field of 0.1 T. The solid line represents a fit of the data with $S = 7$, $g = 2.00(2)$ and $J = +1.6$ cm^{-1}.

This journal is © The Royal Society of Chemistry 2007

Using the program MAGPACK[29] and employing the Hamiltonian in eqn (1):

$$\mathcal{H} = -2J(\hat{s}_1 \cdot \hat{s}_2 + \hat{s}_1 \cdot \hat{s}_{2'}) \quad (1)$$

allowed us to satisfactorily simulate the data with the parameters $J = +1.6$ cm^{-1} and $g = 2.02$ (Fig. 3). The ground state of the complex was found to be $S = 7$, with $S = 6$ and $S = 5$ excited states 4.5 cm^{-1} and 9.0 cm^{-1} above the ground state, respectively. The data can also be satisfactorily simulated employing a $2J$ model and assuming an additional exchange (J_2) between the two peripheral Mn(II) ions with the parameters $J = +1.35$ cm^{-1}, $J_2 = -0.30$ cm^{-1} and $g = 2.03$, but there is no significant enhancement from the $1J$ model.

In order to further verify the magnitude of the spin ground state for complex **1**, magnetisation data were collected in the ranges 10–70 kG and 1.8–6.0 K and these are plotted as reduced magnetisation ($M/N\mu_B$) *vs.* H/T in Fig. 4. For a complex entirely populating the ground state and experiencing no zero-field splitting, the observed isofield lines should superimpose and saturate at a value ($M/N\mu_B$) equal to gS. The fitting of the experimental data with an axial ZFS plus Zeeman Hamiltonian[30] (eqn (2)) over the whole field and temperature range afforded the parameters: $S = 7$, $g = 1.90$, $D = -0.17$ cm^{-1}; whilst fitting only the low temperature (2–4 K) high field (50–70 kG) data afforded the best fit parameters of $S = 7$, $g = 1.93$, $D = -0.23$ cm^{-1}.

$$\mathcal{H} = D(\hat{S}_z^2 - S(S+1)/3) + \mu_B g H \hat{S} \quad (2)$$

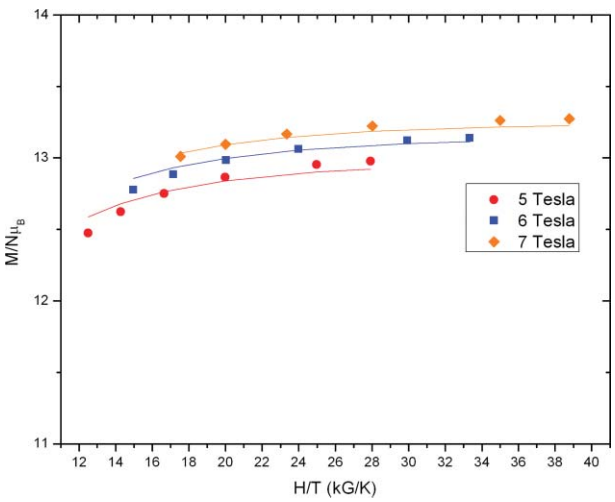

Fig. 4 Plot of reduced magnetisation ($M/N\mu_B$) *vs.* H/T for complex **1**. The solid lines are fits of the data to an $S = 7$ state with $g = 1.93$ and $D = -0.23$ cm^{-1} in a field range of 50–70 kG.

Ac susceptibility

In an ac susceptibility experiment, a weak field (here 3.5 G) oscillating at a particular frequency is applied to a sample to probe the dynamics of the magnetisation relaxation. In-phase (χ_M') and out-of-phase (χ_M'') data were collected on a microcrystalline sample of **1** in the 2–8 K range at four frequencies from 50 to 1000 Hz. If the magnetisation vector can relax fast enough to keep up with the oscillating field there is no out-of-phase susceptibility signal (χ_M''), and the in-phase susceptibility (χ_M') is equal to the dc susceptibility. However, if the barrier to magnetisation relaxation is significant compared to thermal energy, there is a non-zero χ_M'' signal and the in-phase signal decreases. In addition, the χ_M'' signal will be frequency dependent. For complex **1**, the $\chi_M'T$ signal displays little or no frequency dependence (ESI† Fig. SI1), and no out-of-phase (χ_M'') signal is observed down to 1.8 K. Frequency-dependent signals are suggestive of the superparamagnetic-like slow relaxation of a SMM. The $\chi_M'T$ data also provide support for the conclusion from the dc measurements that complex **1** possesses an $S = 7$ ground state: extrapolation of the $\chi_M'T$ plot to 0 K (from above 4 K) gives a value of ~24 cm^3 K mol^{-1}. A well isolated ground state (*vs.* kT) would be expected to be 100% populated at these temperatures and thus the $\chi_M'T$ value would be expected to be temperature independent. A sloping $\chi_M'T$ *versus* T plot is indicative of low-lying excited states whose changing population with temperature affects the observed $\chi_M'T$. In the majority of (antiferromagnetic) complexes the $\chi_M'T$ value tends to decrease with decreasing temperature, consistent with low-lying excited states with S values greater than that of the ground state. As these states become de-populated the $\chi_M'T$ value approaches that corresponding to 100% population of the ground state. For complex **1**, however, the $\chi_M'T$ value is increasing with decreasing temperature, suggesting the presence of low-lying excited states with smaller S values than the ground state. Thus, as they become de-populated the $\chi_M'T$ value increases to that of the ground state. This is as expected for a molecule exhibiting weak intramolecular ferromagnetic exchange (and hence a ground state equal to the maximum possible S) with $S = 6$ and $S = 5$ low-lying excited states. However, it is important to point out that such frequency-dependent signals do not by themselves prove the presence of SMM behaviour, and nor does their absence disprove it. Indeed there are now several examples of molecules, which despite displaying out-of-phase χ_M'' signals do not display SMM behaviour;[31] and here we show complex **1** to be an SMM despite the complete lack of an out-of-phase signal. The only conclusive proof of single-molecule magnetism behaviour comes from the presence of temperature and sweep-rate dependent hysteresis loops in magnetisation *versus* field studies.

Single crystal micro-SQUID measurements

In order to obtain more information about the magnetisation relaxation of complex **1**, dc magnetisation decay data were collected on a single crystal of **1**·Et_2O·2MeCN using a micro-SQUID apparatus.[18] First a large dc field of 1.4 T was applied to the sample at 5 K to saturate the magnetisation in one direction, and the temperature lowered to a specific value between 1.8 and 0.04 K. When the temperature was stable, the field was swept from 1.4 T to 0 T at a rate of 0.14 T s^{-1} and the magnetisation in zero field measured as a function of time. These data were then used to construct an Arrhenius plot which is shown in Fig. 5. The fit of the thermally activated region gave $\tau_0 = 8 \times 10^{-7}$ s and $U_{eff} = 9$ K. Fig. 5 also presents typical magnetisation (M) *vs.* applied dc field measurements on complex **1**·Et_2O·2MeCN at a field sweep rate of 0.002 T s^{-1}. Hysteresis loops are observed, whose coercivity is strongly temperature and sweep rate dependent, increasing with decreasing temperature and increasing field sweep rate, as expected for the superparamagnetic-like behaviour of a SMM. Hysteresis is observed up to at least 0.5 K at a 2 mT s^{-1} sweep rate.

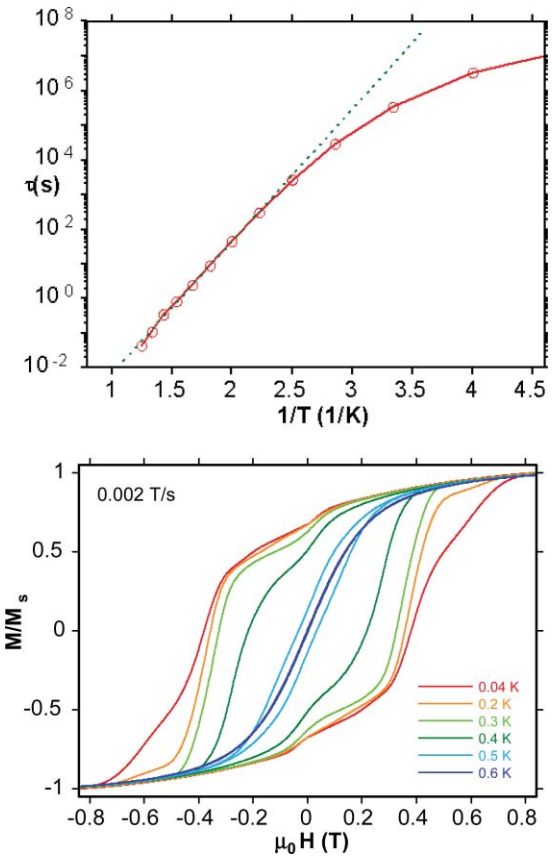

Fig. 5 Plot of relaxation time (τ) *versus* $1/T$ for complex **1**·Et_2O·2MeCN using dc magnetisation decay data (top). The dashed line is a fit of the data to the Arrhenius equation. magnetisation hysteresis loops for a single crystal of **1**·Et_2O·2MeCN (bottom), showing the temperature dependence at a fixed sweep rate of 2 mT s^{-1}. The field was aligned parallel to the easy axis.

The hysteresis loops also show the step-like features at periodic field values that equate to increased magnetisation relaxation, indicative of quantum tunneling of magnetisation (QTM) between the $\pm M_s$ levels on opposite sides of the anisotropy barrier. The separation between the steps is related to D by the equation $\Delta H = |D|/g\mu_B$. Measurement of the step positions for complex **1** afford an average field separation of ~0.22 T and thus a $|D|/g$ value of ~0.10 cm^{-1}. Assuming $g = 2.00$, this corresponds to a $|D|$ value of approximately 0.20 cm^{-1}, in excellent agreement with that obtained from the dc magnetisation measurements.

EPR spectroscopy

Powder samples of **1** give rich EPR spectra below *ca.* 50 K, with resolution of fine structure arising from the ZFS of the $S = 7$ ground state. The fine structure splitting of 0.1–0.2 T observed in the 5 K Q-band spectrum (Fig. 6) suggests a ground state $|D| \approx 0.1$–0.2 cm^{-1}, but the spread of the spectrum over the entire magnetic field range necessitates higher frequency and field measurements. Variable temperature W-band spectra are characteristic of a high spin ground state with axial or near-axial symmetry (Fig. 7). At *ca.* 20 K the spectrum is dominated by the perpendicular manifold with a spacing of *ca.* 0.15 T (although this is not regular across the spectrum). On cooling the sample,

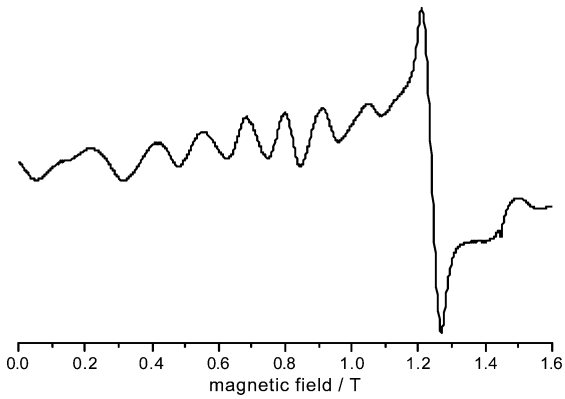

Fig. 6 Q-Band EPR spectrum on a microcrystalline sample of **1** at 5 K.

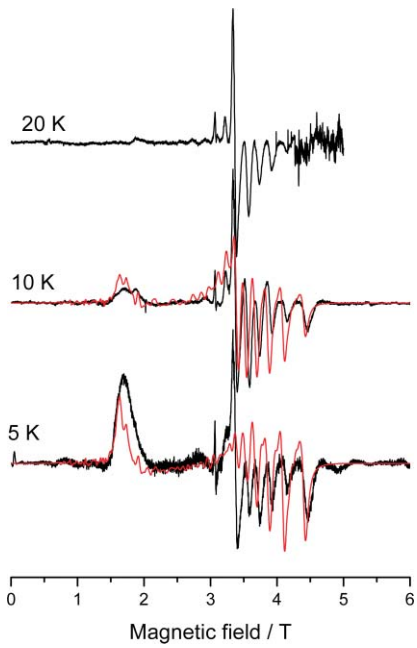

Fig. 7 W-Band EPR spectra of a restrained microcrystalline sample of **1** (black), with simulations based on strong exchange limit Hamiltonian (**2**) and an additional $B_4^0\hat{O}_4^0$ term, with $S = 7$, $D = -0.14$ and $B_4^0 = +1.5 \times 10^{-5}$ cm^{-1}.

the parallel manifold becomes more obvious with the lowest field transitions (*ca.* 1.8 T) increasing in intensity with decreasing temperature, as does the highest field perpendicular component at 4.46 T. These are due to Boltzmann depopulation effects and are characteristic of a negative D.[32] We initially attempted to simulate the spectra in the strong exchange limit (*i.e.* as an isolated $S = 7$ species) with the axial spin Hamiltonian (2). Fixing D to fit the approximately evenly-spaced progression in the central part of the perpendicular manifold (also where the best resolution is observed) gives $D = -0.14$ cm^{-1} and an isotropic g-value of 2.06. This is in reasonable agreement with $|D|$ estimated from the separation between QTM steps in low temperature M *vs* H loops.

This simple Hamiltonian, including only the axial (second order) ZFS term, gives a good fit to the central part of the spectrum but is inadequate in the wings, with the calculated resonance fields for both the lowest-field parallel and the highest-field perpendicular transitions being too low (see ESI† Fig SI2).

This journal is © The Royal Society of Chemistry 2007

This behaviour can be due to additional, higher order ZFS terms in the Hamiltonian (2), which are allowed up to order $2S$.[33] In order to minimize the number of parameters we have restricted ourselves to adding a single, axial fourth order term $B_4^0\hat{O}_4^0$ where the operator is defined as $35\hat{S}_z^4 - 30S(S+1)\hat{S}_z^2 + 25\hat{S}_z^2 - 6S(S+1) + 3S^2(S+1)^2$. This term effects the position of the outer transitions (*i.e.* between states of large $|M_S|$) strongly and its sign relative to that of D is easily determined. Inclusion of $B_4^0 = +1.5 \times 10^{-5}$ cm^{-1}, which is of the same order of magnitude as found for Mn_{12},[34] now gives good resonance fields for these outer transitions including the uneven spacing in the perpendicular multiplet (Fig. 7). However, the fit to the central part of the perpendicular region is slightly poorer than before. This implies that we need to include other 4th or higher order ZFS terms in the Hamiltonian. Accurate determination of these parameters requires single-crystal measurements, and these detailed studies will be reported later.

The C_{2h} molecular symmetry dictates that one of the principal axes of the D tensor must be along the C_2 (Mn$\cdots$Mn$\cdots$Mn) axis with the other two in the mirror plane. We expect D to be dominated by the single-ion ZFS of the central Mn(III) ion and therefore D_{zz} to be approximately aligned along the Mn(III) Jahn Teller distortion axis (Mn1$\cdots$O31) which lies in the mirror plane. Note that although C_{2h} does not impose axial EPR symmetry, introduction of rhombic ZFS terms (E, *etc.*) does not improve the simulations, hence we have restricted ourselves to axial symmetry.

Both Wilson *et al.*[35] and Accorsi *et al.*[36] have recently highlighted that effective higher order fine structure effects can arise from mixing of the cluster spin multiplets ("S-mixing").[37] Any such mixing (implying non-zero off-diagonal matrix elements connecting the different S states) will be inversely proportional to the energy separation between the states (a function of J). Given the small $|J| = 1.6$ cm^{-1} determined for complex **1** [using the isotropic exchange Hamiltonian (1)] we investigated whether similar effects could be in operation here. Hence, we have also calculated EPR spectra using a full interaction Hamiltonian:

$$\mathcal{H} = \sum -2J\hat{s}_i.\hat{s}_j + \sum \mu_B \boldsymbol{g}.B.\hat{s}_i + \sum \hat{s}_i.\boldsymbol{d}_i.\hat{s}_i \qquad (3)$$

where $\hat{s}_i$ are the local (single ion) spin operators and $\boldsymbol{d}_i$ are the local ZFS tensors. In order to reduce the number of variables we have made several approximations: (i) that $d(Mn^{II}) = 0$, (ii) that $d(Mn^{III})$ is axial and co-linear with the cluster ZFS axes, (iii) that the dipolar and anisotropic exchange terms $d(Mn^{II}\cdots Mn^{III})$ are nil, and (iv) an isotropic $g = 2.06$ for all ions. Approximations (i)–(iii) amount to saying that the ground state ZFS arises entirely from the single-ion ZFS of the Mn(III) ion. While clearly an approximation, d of the Jahn Teller distorted Mn(III) ion is typically several cm^{-1} (with d_{zz} along the distortion axis) while that of Mn(II) is typically very small. In order to test the limits of the assumption we have estimated the projections of these terms onto the $S = 7$ ground state ZFS tensor ($\boldsymbol{D}$), in the strong exchange limit, by standard methods.[38] We obtain: $D = 0.220d(Mn^{II}) + 0.066d(Mn^{III}) + 0.286d(Mn^{II}\cdots Mn^{III})$. With a typical value of $|d(Mn^{II})| = 0.05$ cm^{-1} and a value of $d(Mn^{II}\cdots Mn^{III}) = -0.03$ cm^{-1} calculated in the dipolar approximation (oriented along the Mn$\cdots$Mn vector), these interactions account for only 1–10% of D depending on the sign and orientation of $d(Mn^{II})$.

With these approximations, leaving two free parameters $d(Mn^{III})$ and J, eigen-vectors and -values of Hamiltonian (3) were determined by diagonalisation of the full 180 × 180 matrix and the EPR spectra calculated using methods described recently by Piligkos.[30] Fig. 8 shows the effect of decreasing J for a fixed value of $d(Mn^{III}) = -2.3$ cm^{-1} on the calculated 10 K W-band spectrum. With $J = +10$ cm^{-1} the calculated spectrum is very similar to that calculated with Hamiltonian (2) with only D included, with regular spacing of the parallel and perpendicular progressions. As J is decreased, becoming similar in magnitude to $d(Mn^{III})$, similar effects are seen as for introducing the B_4^0 parameter to (2). The bottom panel of Fig. 8 shows the simulation with Hamiltonian (3) and $J = +1.6$ and $d(Mn^{III}) = -2.3$ cm^{-1} together with the experimental 10 K spectrum, the former parameter being that derived from the (isotropic) fit to the magnetic susceptibility data. We do not offer these as definitive values—clearly it is possible to play off the various terms in Hamiltonian (3) against each other—but they serve to illustrate that the 4th order behaviour of the ground state ZFS of **1** arises from the conditions $|J| \approx d(Mn^{III})$ and hence there is a breakdown of the strong exchange limit. Unambiguous determination of the terms in (3) would require synthesis of specific diamagnetic ion substituted complexes, *e.g.* $\{Zn^{II}Mn^{III}Zn^{II}\}$ and $\{Mn^{II}Ga^{III}Mn^{II}\}$.

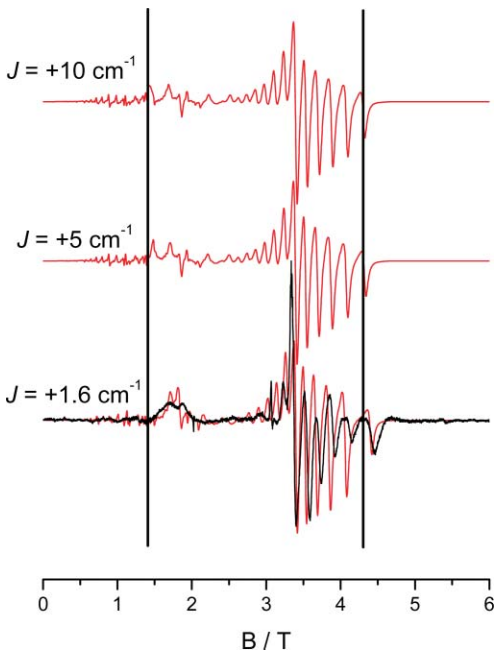

Fig. 8 Effect of varying J on the calculated 10 K W-band EPR spectra (red), using a full interaction Hamiltonian and diagonalising the full 180 × 180 matrix. The vertical lines highlight the shifts in the resonance fields of the lowest-field parallel and highest-field perpendicular transitions as J becomes smaller with respect to $d(Mn^{III})$. Black: experimental 10 K spectrum of **1**.

Computational studies

Density functional calculations of spin Hamiltonian parameters of polynuclear transition metal complexes have become more prevalent in the last decade or so, due to the *relative* success of DFT in the estimation and modelling of experimentally observed magnetic properties. The broken symmetry model, developed by Noodleman, has been particularly successful in the estimation of

the magnetic exchange interactions in dinuclear and polynuclear complexes using HF or DFT methods.[39] The main advantage of this method is that only the energies of single determinants are needed to approximate the energies of the whole spin manifold. For binuclear complexes the approach is straightforward—the J values are related to the energy difference between the high spin state and the broken symmetry state. For polynuclear complexes with several different exchange interactions the calculation of several spin configurations is required, with the energy difference between them then related to the J values by a pairwise interaction model.[40]

The exchange coupling constant, J, has been calculated on the full structure of **1**. The calculations have also been performed on a simplified model complex, $[Mn_3(Hcht)_2(NH_3)_8]^{3+}$ (**2**). Using the broken symmetry formalism to estimate the energy of the low spin states and employing the pairwise exchange model gives the isotropic exchange $J = +3.5\ cm^{-1}$ (Mn(III)–Mn(II)). In comparison to the experimental fit, the sign of the exchange is reproduced but the magnitude is overestimated. Calculations have also been performed in order to obtain an estimate of the interaction between the two peripheral Mn(II) ions. Conventionally this exchange would be considered small enough to be neglected, but in **1** the Mn(III) ion bisects the two Mn(II) ions and its empty orbitals may play a role in mediating an exchange between the two Mn(II) ions—especially so since the distance between the two Mn(II) ions is rather short (6.23 Å). DFT calculations afford J' (Mn(II)–Mn(II)) = $+1.0\ cm^{-1}$; larger than that obtained from the experimental simulation (by $1.3\ cm^{-1}$) and of the wrong sign (ferromagnetic). The same calculations performed on **2** yield $J = +5.0\ cm^{-1}$ and $J' = +0.5\ cm^{-1}$.

The spin density plot of the $S = 7$ state of **1** is shown in Fig. 9. The spin densities are +3.88 for the central Mn(III) ion and +4.77 for the peripheral Mn(II) ions. The positive spin density on the N atoms coordinated to the peripheral Mn(II) ions indicates that spin delocalisation predominates; while for the central Mn(III) ion spin delocalisation predominates along the Jahn–Teller axis and spin polarisation predominates on the equatorial plane. A similar mixed spin-distribution mechanism for Mn(III) ions was reported for the complex $[Mn^{III}{}_3O(bta)_6F_3]^{2+}$.[41]

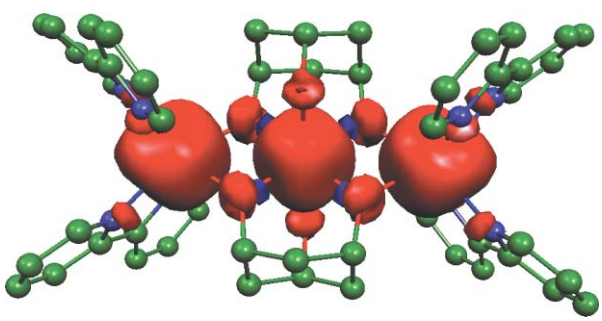

Fig. 9 Spin density plot of the $S = 7$ state of complex **1**. Red represents positive spin density; blue represents negative spin density.

Conclusions

In conclusion, use of the tripodal ligand H_3cht has produced an unusual trinuclear manganese complex containing one Mn(III) ion and two Mn(II) ions that are coupled ferromagnetically to give a spin ground state of $S = 7$. The observed anisotropy is rather small, and considerably smaller than that seen for mononuclear Mn(III) complexes. The result is the absence of an out-of-phase ac susceptibility signal down to 1.8 K. W-Band (94 GHz) EPR measurements on restrained powdered crystalline samples confirm the $S = 7$ ground state and determine the ground state zero-field splitting (ZFS) parameters of $D = -0.14\ cm^{-1}$ and $B_4{}^0 = +1.5 \times 10^{-5}\ cm^{-1}$. The apparent 4th order behaviour is due to a breakdown of the strong exchange limit approximation ($J \approx d$, the single-ion ZFS). Complex **1** displays the temperature and sweep rate dependent hysteresis loops diagnostic of a SMM and is thus the first example of a trinuclear SMM, the first example of a Mn SMM containing only one Mn(III) ion, the second smallest SMM reported and one of the smallest clusters to show QTM.

Acknowledgements

We thank Lloyd's of London Tercentenary Foundation, The Leverhulme Trust, the EPSRC, the EC (MAGMANet), and the Marie Curie Intra-European Fellowships for funding.

Notes and references

1 R. Sessoli, H.-L Tsai, A. R. Schake, S. Wang, J. B. Vincent, K. Folting, D. Gatteschi, G. Christou and D. N. Hendrickson, *J. Am. Chem. Soc.*, 1993, **115**, 1804.
2 R. Sessoli, D. Gatteschi, A. Caneschi and M. A. Novak, *Nature*, 1993, **365**, 141.
3 G. Christou, D. Gatteschi, D. N. Hendrickson and R. Sessoli, *MRS Bull.*, 2000, **25**, 66.
4 G. Aromí and E. K. Brechin, *Struct. Bonding*, 2006, **122**, 1.
5 R. Bircher, G. Chabousant, C. Dobe, H. U. Güdel, S. T. Ochsenbein, A. Sieber and O. Waldmann, *Adv. Funct. Mater.*, 2006, **16**, 209.
6 S. M. J. Aubin, M. W. Wemple, D. M. Adams, H.-L. Tsai, G. Christou and D. N. Hendrickson, *J. Am. Chem. Soc.*, 1996, **118**, 7746.
7 J. R. Friedman, M. P. Sarachik, J. Tejada and R. M. Ziolo, *Phys. Rev. Lett.*, 1996, **76**, 3830.
8 L. Thomas, F. Lionti, R. Ballou, D. Gatteschi, R. Sessoli and B. Barbara, *Nature*, 1996, **383**, 145.
9 D. Gatteschi and R. Sessoli, *Angew. Chem., Int. Ed.*, 2003, **42**, 268.
10 W. Wernsdorfer and R. Sessoli, *Science*, 1999, **284**, 133.
11 M. N. Leuenberger and D. Loss, *Nature*, 2001, **410**, 789.
12 C. J. Milios, A. Vinslava, S. Moggach, S. Parsons, G. Christou, S. P. Perlepes, W. Wernsdorfer and E. K. Brechin, *J. Am. Chem. Soc.*, 2007, **129**, 2754.
13 E. K. Brechin, *Chem. Commun.*, 2005, 5141.
14 L. F. Jones, A. Batsanov, E. K. Brechin, D. Collison, M. Helliwell, T. Mallah, E. J. L. McInnes and S. Piligkos, *Angew. Chem., Int. Ed.*, 2002, **41**, 4318.
15 R. Shaw, I. S. Tidmarsh, R. H. Laye, B. Breeze, M. Helliwell, E. K. Brechin, S. L. Heath, M. Murrie, S. T. Ochsenbein, H.-U. Güdel and E. J. L. McInnes, *Chem. Commun.*, 2004, 1418.
16 J. P. Corden, W. Errington, P. Moore, M. G. Partridge and M. G. H. Wallbridge, *J. Chem. Soc., Dalton Trans.*, 1999, 2647.
17 (*a*) R. T. W. Scott, S. Parsons, M. Murugesu, W. Wernsdorfer, G. Christou and E. K. Brechin, *Chem. Commun.*, 2005, 2083; (*b*) for a complete list all known SMMs to mid-2005 including other trimetallic SMMs please see reference 4 and for example C. Kachi-Terajima, H. Miyasaka, A. Saitoh, N. Shirakawa, M. Yamashita and R. Clérac, *Inorg. Chem.*, 2007, **46**, 5861; D. Li, R. Clérac, S. Parkin, G. Wang, G. T. Yee and S. M. Holmes, *Inorg. Chem.*, 2006, **45**, 5251; (*c*) S. R. Cooper and M. J. Calvin, *J. Am. Chem. Soc.*, 1977, **99**, 6623.
18 W. Wernsdorfer, *Adv. Chem. Phys.*, 2001, **118**, 99.
19 C. H. J. Jacobsen, E. Pedersen, J. Villadsen and H. Weihe, *Inorg. Chem.*, 1993, **32**, 1216.
20 G. M. Sheldrick, *SHELXL-97, Program for refinement of crystal structures*, University of Göttingen, Germany, 1997.
21 P. T. Beurskens, G. Beurskens, W. P. Bosman, R. de Gelder, S. Garcia-Granda, R. O. Gould, R. Israel and J. M. M. Smits, *The DIRDIF96*

 This journal is © The Royal Society of Chemistry 2007

Program System, Technical Report of the Crystallography Laboratory, University of Nijmegen, The Netherlands, 1996.
22 *Jaguar 5.0*, Schrodinger Inc, Portland, OR, 2003.
23 A. D. Becke, *Phys. Rev. A*, 1988, **38**, 3098.
24 C. T. Lee, W. T. Yang and R. G. Parr, *Phys. Rev. B*, 1988, **37**, 785.
25 A. D. Becke, *J. Chem. Phys.*, 1993, **98**, 5648.
26 A. Schafer, H. Horn and R. Ahlrichs, *J. Chem. Phys.*, 1992, **97**, 2571.
27 A. Schafer, C. Huber and R. Ahlrichs, *J. Chem. Phys.*, 1994, **100**, 5829.
28 E. Ruiz, J. Cano, S. Alvarez and P. Alemany, *J. Comput. Chem.*, 1999, **20**, 1391.
29 (*a*) J. J. Borrás-Almenar, J. M. Clemente-Juan, E. Coronado and B. S. Tsukerblat, *Inorg. Chem.*, 1999, **38**, 6081; (*b*) J. J. Borrás-Almenar, J. M. Clemente-Juan, E. Coronado and B. S. Tsukerblat, *J. Comput. Chem.*, 2001, **22**, 985.
30 S. Piligkos, E. Bill, D. Collison, E. J. L. McInnes, G. A. Timco, H. Weihe, R. E. P. Winpenny and F. Neese, *J. Am. Chem. Soc.*, 2007, **129**, 760.
31 See for example: A. Mishra, W. Wernsdorfer, S. Parsons, G. Christou and E. K. Brechin, *Chem. Commun.*, 2005, 2086.
32 A.-L. Barra, L.-C. Brunel, D. Gatteschi, L. Pardi and R. Sessoli, *Acc. Chem. Res.*, 1998, **31**, 460.
33 A. Abragam and B. Bleaney, *Electron Paramagnetic Resonance of Transition Ions*, Dover, New York, 1986.
34 (*a*) A.-L. Barra, D. Gatteschi and R. Sessoli, *Phys. Rev. B*, 1997, **56**, 8192; (*b*) S. Hill, R. S. Edwards, S. I. Jones, D. S. Dalal and J. M. North, *Phys. Rev. Lett.*, 2003, **90**, 217204.
35 A. Wilson, J. Lawrence, E.-C. Yang, M. Nakano, D. N. Hendrickson and S. Hill, *Phys. Rev. B*, 2006, **74**, 140403.
36 S. Accorsi, A.-L. Barra, A. Caneschi, G. Chastanet, A. Cornia, A. C. Fabretti, D. Gatteschi, C. Mortalò, E. Olivieri, F. Parenti, P. Rosa, R. Sessoli, L. Sorace, W. Wernsdorfer and L. Zobbi, *J. Am. Chem. Soc.*, 2006, **128**, 4742.
37 S. Carretta, E. Liviotti, N. Magnani, P. Santini and G. Amoretti, *Phys. Rev. Lett.*, 2004, **92**, 207205.
38 A. Bencini and D. Gatteschi, *EPR of Exchange Coupled Systems*, Springer-Verlag, Berlin, 1990.
39 L. J. Noodleman, *Chem. Phys.*, 1981, **74**, 5737.
40 E. Ruiz, S. Alvarez, A. Rodriguez-Fortea, P. Alemany, Y. Pouillon, and C. Massobiro, in *Magnetism: Molecules to Materials II*, ed. J. S. Miller and M. Drillon, Wiley-VCH, Weinheim, 2001, p. 227.
41 L. F. Jones, G. Rajaraman, J. Brockman, M. Murugesu, J. Raftery, S. J. Teat, W. Wernsdorfer, G. Christou, E. K. Brechin and D. Collison, *Chem.–Eur. J.*, 2004, **10**, 5180.